Materials Science & Engineering B 244 (2019) 65–71

Contents lists available at ScienceDirect

Materials Science & Engineering B

journal homepage: www.elsevier.com/locate/mseb

Structure and thermoelectric properties of calcium doped Sr_2TiCoO_6 double perovskites

Sudha, Mandvi Saxena, Kantesh Balani, Tanmoy Maiti*

Department of Materials Science and Engineering, Indian Institute of Technology Kanpur, UP 208016, India

ARTICLE INFO

Keywords:
Double perovskites
Thermoelectric
Polaron hopping
Oxides

ABSTRACT

Present work investigates the effect of calcium doping on the structure and thermoelectric properties of Sr_2TiCoO_6 (STC) double perovskite. Environmentally friendly rare earth free $Ca_xSr_{2-x}TiCoO_6$ ($0.0 \leq x \leq 0.3$) (CSTC) ceramics were synthesized using solid state synthesis route. CSTC ceramics were found to possess a cubic crystal structure with $Pm\bar{3}m$ space group as confirmed by Rietveld refinement of XRD data. Microstructure analysis was carried out by SEM and energy dispersive x-ray spectroscopy. The temperature dependent electrical conductivity and thermopower of these oxides showed the semiconductor to metal transition at around 700 K. X-ray photoelectron spectroscopy (XPS) confirmed the presence of multiples oxidation states of Co and Ti creating defect sites in these oxides. CSTC ceramic samples exhibited positive Seebeck coefficient implying p-type behavior. Charge transport mechanism of all the CSTC samples was found to be governed by small polaron hopping model.

1. Introduction

Thermoelectric power generation, which produces electricity from waste heat is considered as the key technology to resolve the issue of global warming as well as the energy problem. Thermoelectric materials convert heat energy directly into the electrical energy without any emission of greenhouse gases [1–5]. The performance of thermoelectric devices is measured by dimensionless figure of merit which can be written as

$$ZT = \frac{S^2\sigma}{\kappa}T \quad (1)$$

where S is the Seebeck coefficient, σ is electrical conductivity, T is temperature and k is thermal conductivity. Further thermal conductivity can be expressed as $k = k_e + k_l$, Where k_e is carrier thermal conductivity due to electron and hole and k_l is the lattice thermal conductivity due to phonon. A good thermoelectric material should possess high ZT value, which can be attained when the material has large Seebeck coefficient, high electrical conductivity and low thermal conductivity. Slack [6] propounded the 'phonon glass and electron crystal' (PGEC) model for achieving the high ZT values. This model suggests that ideal thermoelectric material should have crystal like electronic property and amorphous material such as glass like thermal conductivity which are not easy to achieve in a single compound [7]. Over the past decades, several new material systems were designed based on the PGEC model demonstrating good ZT values. Especially chalcogenides like Bi_2Te_3 [8], PbTe [9], SnSe [10] etc., are considered as state-of-the-art thermoelectric materials because of their high ZT values ($ZT \geq 1$) [7]. However, these materials are not appropriate for use at high temperature ($T \geq 700$ K), because their constituent elements easily melt, decompose or vaporize. Since the discovery of layered cobaltites with promising ZT value (~0.3 at 1000 K) [11], oxides [12–17] are considered as viable option due to low processing cost, better thermal and chemical stability. However, their ZT values are much lower compared to chalcogenides.

Recently, double perovskites showed promises as high temperature thermoelectric material. The general formula for double perovskite oxides is $A_2B'B''O_6$, where A is the alkaline earth elements; B' and B'' are transition metals. In these double perovskite oxides B' and B'' are arranged in octahedral manner with six oxygen atoms in the form of $B'O_6$ and $B''O_6$. These materials showed various attractive properties for example ferroelectricity [18], colossal magnetoresistance [19], Mott insulators [20], high Tc superconductivity [21], etc. Additionally, these double perovskites show half metallic ground states where conduction electrons are fully spin polarized due to their extraordinary electronic structure [22,23]. Recently, authors [24–29] investigated the high temperature thermoelectric properties of double-perovskite oxides $Sr_2TiB'O_6 (B' = Co, Mo, Fe)$. We [27–29] reported that the de-coupling of phonon glass and electron crystal behavior is possible in Ba doped Sr_2TiCoO_6 (STC) oxide materials resulting reasonable ZT values (~0.3)

* Corresponding author.
E-mail address: tmaiti@iitk.ac.in (T. Maiti).

https://doi.org/10.1016/j.mseb.2019.04.025
Received 28 February 2018; Received in revised form 7 March 2019; Accepted 30 April 2019
Available online 09 May 2019
0921-5107/

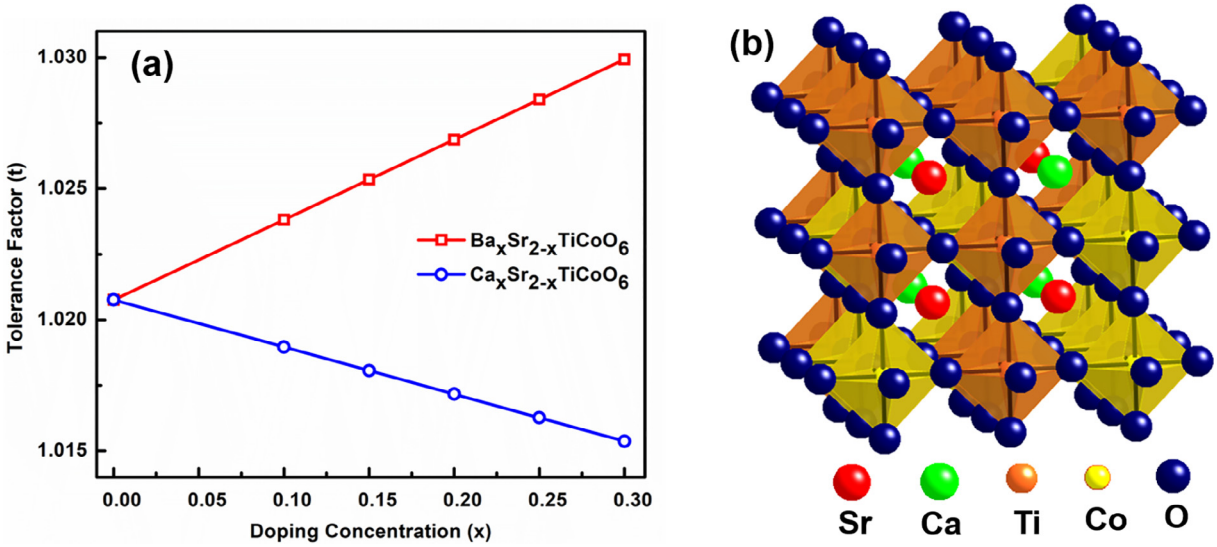

Fig. 1. (a) Tolerance factor of Ba and Ca doped Sr_2TiCoO_6 and (b) Schematic representation of $Ca_xSr_{2-x}TiCoO_6$ double perovskite.

obtained at 1223 K. These $Ba_xSr_{2-x}TiCoO_6$ based double perovskite materials exhibited glass like thermal conductivity (< 0.55 W/mK) at high temperature as a consequence of induced dipolar glassy phase due to relaxor ferroelectric behavior observed in these oxides below room temperature [27]. Meanwhile, in the prior research calcium was proven to be effective constituent or dopant in order to achieve enhanced ZT values in wide range of materials such as layered cobaltites [11,30], oxyselenides [31], perovskites [32] and double perovskites [33]. Goldschmidt tolerance factor [34] is generally used for designing new perovskite materials. The tolerance factor [35] was calculated for Ba and Ca doped $Sr_{2-x}TiCoO_6$ double perovskites using the modified expression for $A'_xSr_{2-x}TiCoO_6 (A' = Ba, Ca)$ given by Eq. (2).

$$t = \frac{\frac{(x)r_{A'} + (2-x)r_{Sr}}{2} + r_O}{\sqrt{2}\left(\frac{r_{Ti} + r_{Co}}{2} + r_O\right)} \quad (2)$$

where, r_O, r_{Sr}, r_{Ti}, r_{co},and $r_{A'}$ are the ionic radii of oxygen, strontium, titanium, cobalt and $A'(Ba\ or\ Ca)$ ions, respectively. It can be seen from Fig. 1 (a) that substitution of Ca in Sr-site of STC double perovskite results the gradual decrease in tolerance factor compared to the increasing trend found in case of Ba doped STC. So, it was intriguing to investigate the effect of Ca doping in STC. In the current work, we studied the thermoelectric properties of Ca doped Sr_2TiCoO_6 (STC) double perovskite structure as shown schematically in Fig. 1(b). To the best of our knowledge this is the first report of thermoelectric properties of $Ca_xSr_{2-x}TiCoO_6$ (CSTC) double perovskites. Polycrystalline samples of CSTC ($0.0 \le x \le 0.3$) were synthesized by solid state reaction route, and its thermoelectric properties were measured in the temperature range from 300 K to 1050 K. All the CSTC ceramic samples showed positive Seebeck coefficient suggesting that it is a p-type thermoelectric material.

2. Experimental procedure

Double perovskite $Ca_xSr_{2-x}TiCoO_6$ samples with $0.0 \le x \le 0.3$ were prepared by conventional solid-state reaction method. The stoichiometric compositions of $Ca_xSr_{2-x}TiCoO_6$ were synthesized by mixing the appropriate ratio of raw materials such as, $SrCO_3$ (>99.9% Purity, Sigma Aldrich), $CaCO_3$ (99.95%, Himedia), Co_3O_4 (> 99.7%, Alfa Assar) and TiO_2 (> 99.5% Purity, Sigma Aldrich) in ball mill at 350 rpm for 24 h and ethanol was used as the wetting media. Then mixed CSTC powder was calcined at 1323 K for 10 h in air atmosphere. The agglomerated CSTC powder was ground for obtaining the fine powder. We obtained homogeneous CSTC powder from the planetary micro ball mill (Fritsch®, PULVERISETTE 7 premium Line, Rhineland-Palatinate, Germany) at 600 rpm for 120 min using Zirconia grinding balls (5:2:1 ratio) and ethanol used as wetting media again. Nano milled powder was uniaxially pressed into the pellets by adding 2 wt% PVA (poly vinyl alcohol) binder and sintered in air atmosphere at 1473 K for 12 h. The X-Ray diffraction (XRD) pattern was measured in the 2θ range from 20° to 90° by using PANalytical X'Pert diffractometer with Cu-Kα radiation (λ = 1.5418Å) at 45 kV, 40 mA and step size 0.01. The refinement of the crystal structure was performed by the Rietveld method, using the FULLPROF [36] refinement program. Microstructures of as-sintered samples were taken by scanning electron micrograph (SEM, Carl Zeiss NTS GmbH, EV050, Germany) in secondary electron mode. Energy dispersive x-ray spectroscopy (EDXS) analysis of $Ca_xSr_{2-x}TiCoO_6$ ($0 \le x \le 0.3$) samples were achieved using Bruker SDD-EDS detector. Furthermore, X-Ray photoelectron spectroscopy (XPS) spectra for CSTC samples were measured using the PHI 5000 Versaprobe II. A non-monochromatic Al-Kα radiation source of energy 1486.6 eV was used to excite the electron. The binding energy of Carbon (284.6 eV) was taken as the reference energy for measuring the binding energy for other CSTC elements. The electrical resistivity ρ (Ω-m), and Seebeck coefficient S (μV/K) were simultaneously measured in a helium atmosphere from RT to 1050 K by ZEM-3 M10 apparatus (ULVAC-RICO Inc.) with the step size of 50 K.

3. Result and discussion

X-Ray diffraction (XRD) patterns of $Ca_xSr_{2-x}TiCoO_6$ (CSTC) samples showed no evidence of secondary phase as shown in Fig. 2, which confirmed the single-phase solid solution obtained for all the compositions of CSTC. All the XRD peaks were indexed to the pursuance of perovskite structures as shown in Fig. 2. Further, we carried out the Rietveld analysis of the XRD data by using Fullprof software [36]. The crystal structure was refined by using cubic symmetry with $Pm\bar{3}m$ space group. The peak shape was described by the pseudo-voigt function, which is the mixture of Lorentzian and Gaussian peak shape and the background variation was linearly interpolated. In the Rietveld analysis, parameters such as thermal parameter, background, shape, i.e. FWHM, lattice parameter, zero correction, etc. were varied to obtain the more accurate information about the structure.

Fig. 2(e) shows the observed, calculated, Bragg positions and difference profile of the $Ca_xSr_{2-x}TiCoO_6$ (x = 0.3) composition obtained after refinement of the XRD data. All the compositions showed a good

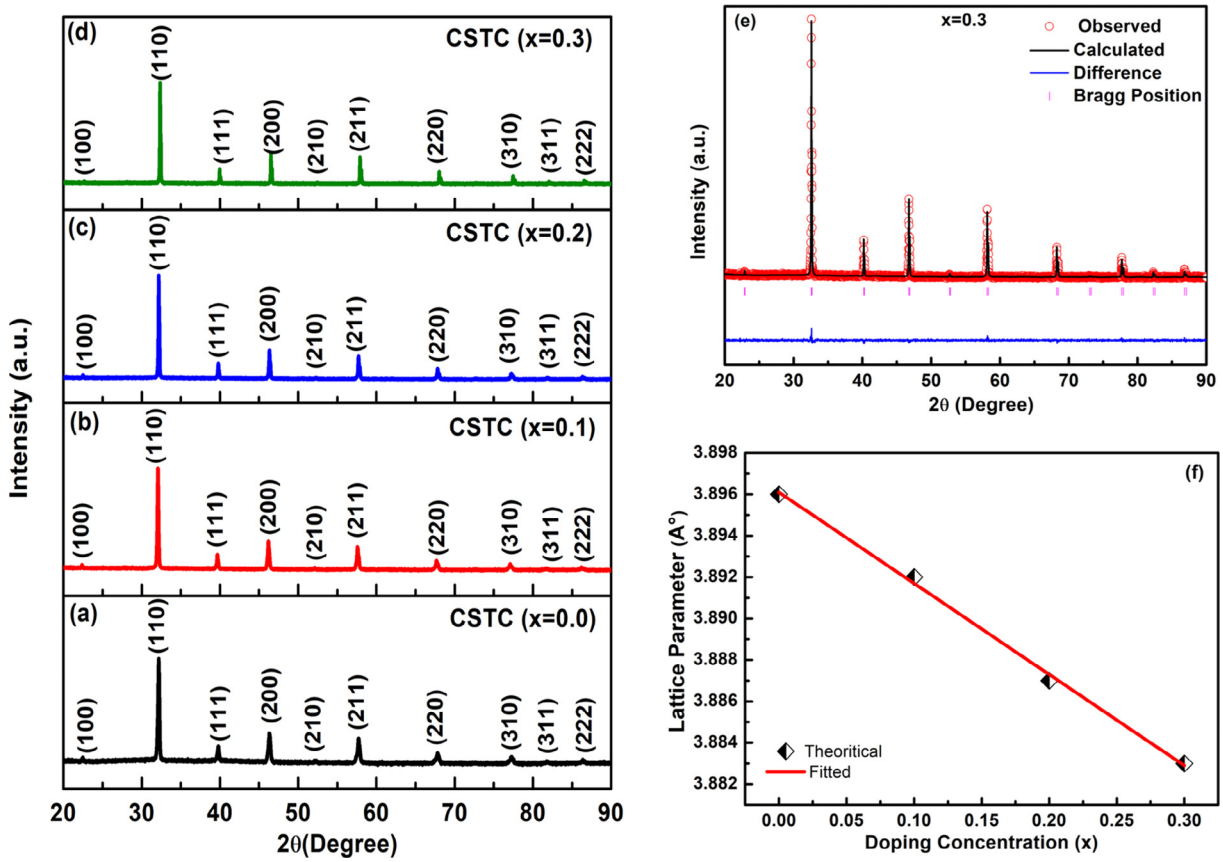

Fig. 2. X-Ray diffraction (XRD) pattern of sintered $Ca_xSr_{2-x}TiCoO_6$ ($0 \le x \le 0.3$), (a) CSTC (x = 0), (b) CSTC (x = 0.1), (c) CSTC (x = 0.2), (d) CSTC (x = 0.3) compositions, (e) Rietveld refinement fitted data of CSTC (x = 0.3) sample with $Pm\bar{3}m$ space group and (f) Variation in lattice parameter with doping concentration (x) of Ca following Vegard's law.

Table 1
Refined structural parameter of $Ca_xSr_{2-x}TiCoO_6$ ($0 \le x \le 0.3$) obtained after Rietveld refinement of XRD data and measured density from Archimedes' principle.

Composition	Lattice Parameter a = b = c (Å)	Volume (Å)^3	R_F Factor	R_B Factor	χ^2	Theoretical Density (g/cm^3)	Measured Density (Archimedes) (g/cm^3)
Sr_2TiCoO_6	3.896(8)	59.171	2.45	2.36	1.04	5.305	4.90 ± 0.03
$Ca_{0.1}Sr_{1.9}CoO_6$	3.892(4)	59.043	3.20	3.28	1.85	5.304	5.04 ± 0.01
$Ca_{0.2}Sr_{1.8}CoO_6$	3.887(5)	58.751	2.13	1.90	1.45	5.316	5.06 ± 0.01
$Ca_{0.3}Sr_{1.7}CoO_6$	3.882(7)	58.535	1.60	1.99	1.38	5.322	4.97 ± 0.03

fit with respect to $Pm\bar{3}m$ space group as evident from low values of χ^2 obtained for all the compositions. All the refinement fitting parameters R_F, R_B, Lattice parameter and χ^2, are listed in Table 1. The lattice parameter for CSTC compositions decreased with the substitution of calcium, which is expected since the ionic radius of Ca^{+2} (1.34 Å) is smaller than Sr^{+2} (1.44 Å) ion. Moreover, CSTC system was found to follow the Vegard's law as evident from the linear relationship between lattice parameter and Ca content in CSTC shown in Fig. 2(f). Theoretical density as well as density measured by Archimedes' principle are presented in Table 1. The density for all CSTC samples were found to be 92–95% of theoretical density.

Fig. 3 shows the microstructure of the as-sintered surfaces of $Ca_xSr_{2-x}TiCoO_6$ ($0.0 \le x \le 0.3$) ceramics, which suggests that all the CSTC samples were well-sintered and highly dense with not much porosity. Grain size of the CSTC samples was calculated by using Image J software [37] and obtained grain size was found to be in the range from 2.5 to 6.1 μm.

Energy dispersive x-ray spectroscopy (EDXS) of $Ca_xSr_{2-x}TiCoO_6$ ($0 \le x \le 0.3$) was carried out to verify the homogeneity of the ceramic. The color elemental mappings of the constituent elements such as Ca, Sr, Ti, Co, and O were acquired on the small area of as-sintered CSTC (x = 0.2) ceramics as shown in Fig. 4. It is apparent that all the elements of CSTC ceramic samples were homogeneously distributed without any sign of phase segregation.

3.1. Thermoelectric properties of $Ca_xSr_{2-x}TiCoO_6$ ($0 \le x \le 0.3$):

Fig. 5 depicts the electrical conductivity (σ) and Seebeck coefficient (S) of $Ca_xSr_{2-x}TiCoO_6$ ($0 \le x \le 0.3$) samples, which were measured in the temperature range from 300 K to 1050 K. Fig. 5 (a) shows the signature of semiconductor ($d\sigma/dT > 0$) to metallic ($d\sigma/dT < 0$) to semiconductor ($d\sigma/dT > 0$) phase transition in the temperature dependent conductivity graph. All the CSTC compounds exhibited the electrical conductivity on the order of ~ 10^2 S/m at room temperature. Temperature-dependent conductivity curve showed a distinct peak corresponding with semiconductor ($d\sigma/dT > 0$) to metal like ($d\sigma/dT < 0$) transition for all $Ca_xSr_{2-x}TiCoO_6$ ($0 \le x \le 0.3$) compositions, similar to what was observed for the pure Sr_2TiCoO_6 double perovskites [25,27]. Ca-doped STC samples also kept up the high temperature semiconductor behavior, which was observed in STC resulting an intermediate metallic like transition between two semiconductor phases.

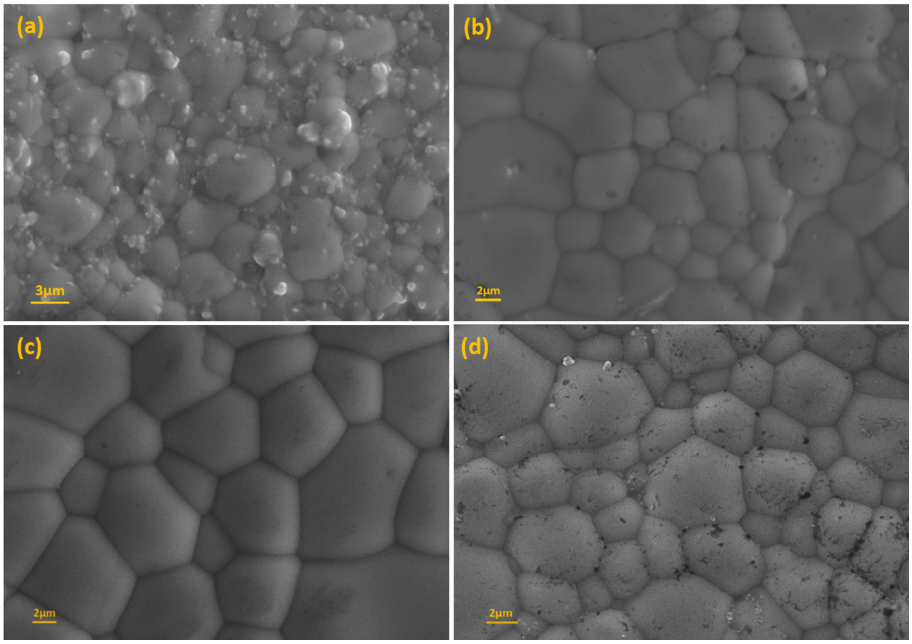

Fig. 3. Scanning electron microscopy (SEM) images of $Ca_xSr_{2-x}TiCoO_6$ ($0 \leq x \leq 0.3$) samples collected in secondary electron mode, (a) CSTC (x = 0), (b) x = 0.1, (c) x = 0.2 and (d) x = 0.3.

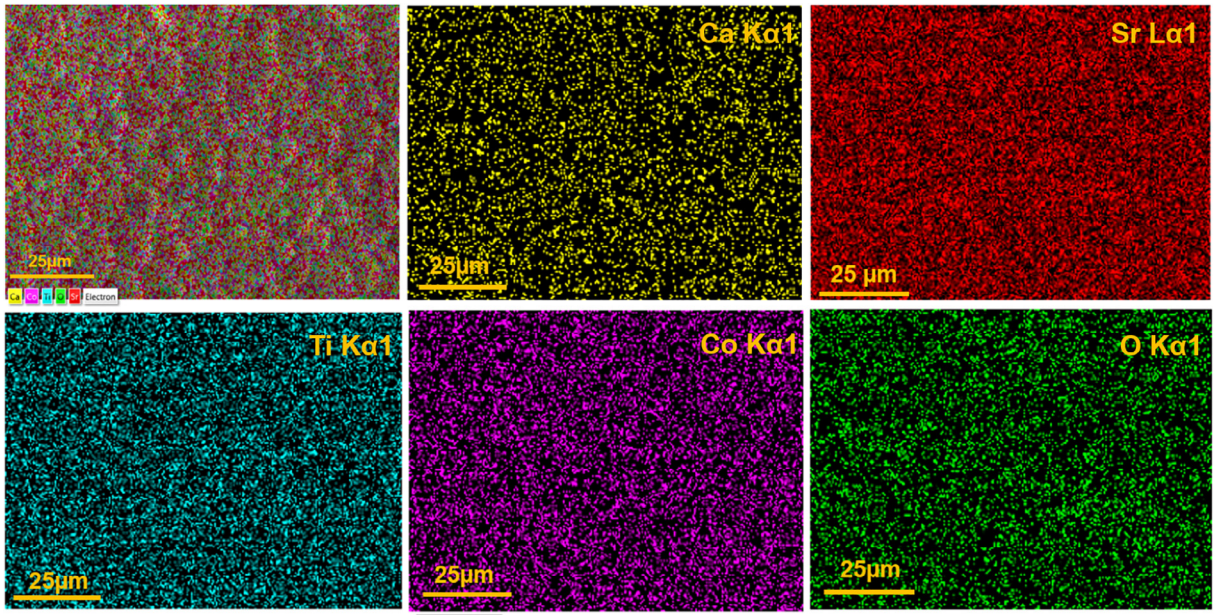

Fig. 4. Energy dispersive x-ray spectroscopy (EDXS) of $Ca_{0.2}Sr_{1.98}TiCoO_6$ sample showing elemental mapping for constituents Ca, Sr, Ti, Co and O.

The maximum electrical conductivity was found to be ~ 2709 S/m at ~760 K for x = 0.1 composition.

The Seebeck coefficient initially decreased with temperature before it started showing increasing trend for all the CSTC ceramic samples as shown in Fig. 5(b). The point of inflection matches with the semiconductor to metal transition temperature observed in conductivity vs temperature curve. The Seebeck coefficient was found to be positive for all the CSTC ceramic samples, which confirmed the p-type transport in the entire temperature range from 300 K to 1050 K. The distinct peak obtained in temperature dependent Seebeck coefficient graph of Ca doped STC needs to be explained with further investigation. At this point, the intermediate metal like transition between two semiconductor phases is proposed to be responsible for the Seebeck coefficient peak.

The source of positive charge carriers in CSTC compounds is attributed to the presence of multivalent cations such as Ti, Co in the B-site of these double perovskites. Ti and Co ion can be present in Ti^{+4}, Ti^{+3} and Co^{+3}, Co^{+2} valence state in the B-site of the double perovskite which has the formal valence of +4. The defect reactions occurred in CSTC compounds can be expressed by Kroger -Vink notation,

$$Co_2O_3 + \frac{1}{2}O_2(g) \overset{2BO_2}{\rightarrow} 2Co_B' + 4O_o^x + 2h \quad (3)$$

$$CoO + \frac{1}{2}O_2(g) \overset{BO_2}{\rightarrow} Co_B'' + 2O_o^x + 2h \quad (4)$$

$$Ti_2O_3 + \frac{1}{2}O_2(g) \overset{2Bo_2}{\rightarrow} 2Ti_B' + 4O_o^x + 2h \quad (5)$$

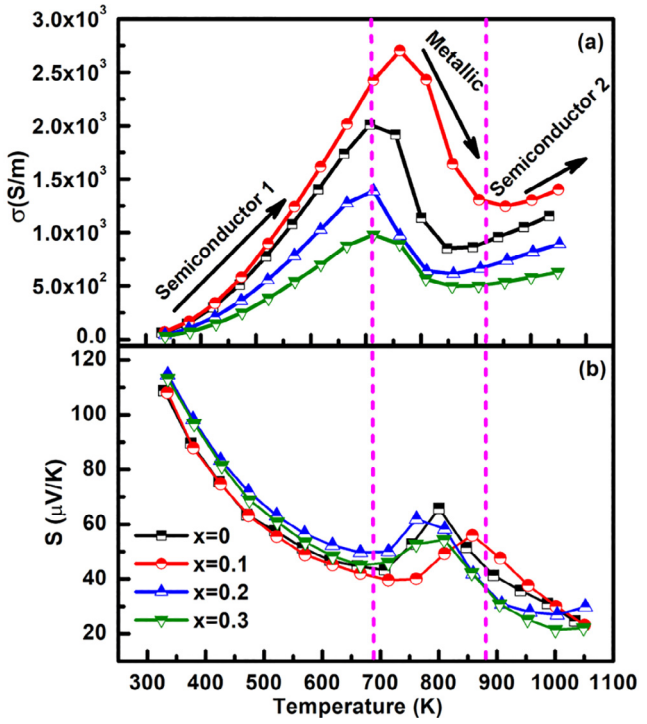

Fig. 5. Temperature dependent (a) Electrical conductivity (σ S/m) and (b) Seebeck coefficient (μV/K) of $Ca_xSr_{2-x}TiCoO_6$ ($0 \le x \le 0.3$) ceramics.

$$TiO_2 \xrightarrow{BO_2} Ti_B^x + 2O_o^x \quad (6)$$

These defect reactions suggest that the presence of Co^{+2}, Co^{+3}, and Ti^{+3} can donate holes in this CSTC systems resulting p-type behavior observed in these double perovskites. No change in the type of charge carriers is expected in Ca doped STC compounds as Ca^{+2} and Sr^{+2} are isovalent.

Furthermore, the oxidation states of multivalent cations such as Co and Ti in these CSTC compounds were confirmed by X-ray photoelectron spectroscopy (XPS). XPS Spectra collected for Co 2p, and Ti 2p are shown in Fig. 6(a) and (b), respectively. The obtained peaks in XPS spectra were fitted using Lorentzian-Gaussian line shape after Tougaard [38] type background correction for $Ca_xSr_{2-x}TiCoO_6$ (x = 0.3) sample. Estimated binding energies are presented in Table 2. All the estimated binding energy values were found to be in good agreement with the previous literature [39,40]. The obtained binding energy difference ($\Delta\beta_E$) i.e. spin orbit splitting energy for Co^{2+} $2p_{1/2} - 2p_{3/2}$ is 15.62 eV which distinguished the presence of high spin Co. $\Delta\beta_E$ for Co^{3+} $2p_{1/2} - 2p_{3/2}$ was estimated as 15.45 eV. We also found the presence of satellite peaks on the higher binding energy side Co $2p_{3/2}$ spectra, which were also observed by earlier researchers [40–44].

Table 2
Binding energy, FWHM, and area percentage of the Co 2p and Ti 2p XPS spectra for $Ca_xSr_{2-x}TiCoO_6$ (x = 0.3) sample.

Element	Spectral Region	Binding Energy (eV)	FWHM (eV)	Area %
Co 2p	2P $_{3/2}$ Co^{2+}	781.45	3.66	29
	2P $_{3/2}$ Co^{3+}	779.80	2.76	23
	2P $_{3/2}$ satellite	785.52	5.0	21
	2P $_{1/2}$ Satellite	789.65	4.0	6.4
	2P $_{1/2}$ Co^{2+}	797.07	2.68	6.4
	2P $_{1/2}$ Co^{3+}	795.25	3.12	14.1
Ti 2p	2P $_{3/2}$ Ti^{2+}	456.61	0.984	15.3
	2P $_{3/2}$ Ti^{3+}	457.11	1.338	33
	2P $_{3/2}$ Ti^{4+}	458.30	2.385	14.2
	2P $_{3/2}$ Satellite	455.49	0.313	0.3
	2P $_{1/2}$$Ti^{2+}$	461.39	1.231	2.1
	2P $_{1/2}$$Ti^{3+}$	462.82	2.492	32.6
	2P $_{1/2}$$Ti^{4+}$	464.91	0.698	1.7
	2P $_{1/2}$ Satellite	465.55	0.482	0.9

Fig. 6 (b) represents Ti 2p XPS spectra for $Ca_xSr_{2-x}TiCoO_6$ (x = 0.3) sample. In our investigation, we found the existence of mixed valence states of Ti^{4+}, Ti^{3+} and Ti^{2+} in the XPS spectra as shown in Table 2. The obtained binding energy for different valence states of Ti were found to be similar to what were reported in the literature [26,45]. Fig. 6(b) shows an asymmetry in the $2p_{3/2}$ peak as well as in $2p_{1/2}$ resulting the multiplet splitting similar to what was reported earlier [46–48]. It is apparent from the estimated area in the fitted XPS curve presented in Table 2 that most of the cobalt existed as Co^{2+}, whereas +3 oxidation state of Ti was dominant over the other valence states. It further validates the occurrence of positive charge carrier, holes due to the presence of Ti^{3+}, Ti^{2+} and Co^{3+}, Co^{2+} in CSTC system as described by the defect reactions mentioned above.

To understand the conduction mechanism of these type of materials, band model may not be suitable. There are lot of defects present in CSTC double perovskite oxides. It is plausible that the charge carriers are localized at ($Co_B^{/}$, $Co_B^{//}$, $Ti_B^{/}$) defect sites. Further, these defect sites create the variation in local electric field as well as lattice strain resulting an energy barrier which needs to be overcome by the charge carriers i.e. holes in this case. The charge carrier requires enough ionization energy to cross the barrier by jumping off from one site to another. Therefore, the small polaron hopping conduction model seems to be more appropriate to deduce the transport behavior of these perovskites-based oxides. Electrical conductivity driven by Small polaron hopping conduction can be expressed by following equation [49–54]

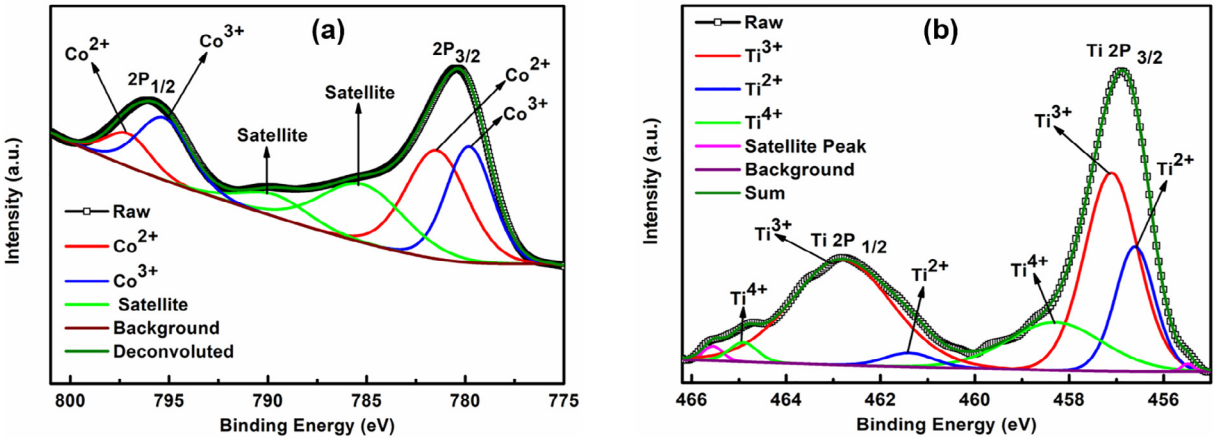

Fig. 6. X-Ray photoelectron spectroscopy (XPS) spectra of (a) Co 2p and (b) Ti 2p peak for $Ca_xSr_{2-x}TiCoC_6$ (x = 0.3) sample.

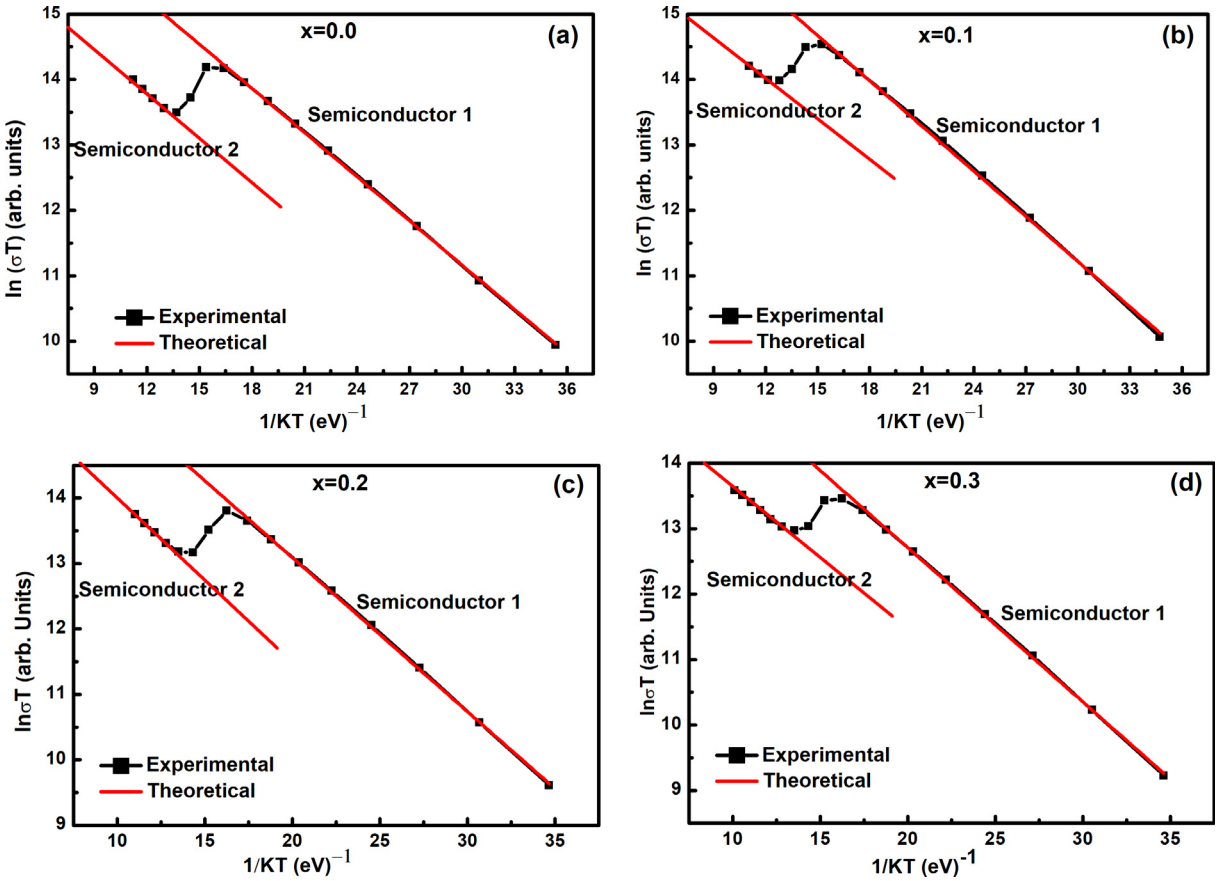

Fig. 7. Plot of ln(σT) vs. $\frac{1}{K_B T}$ for $Ca_xSr_{2-x}TiCoO_6$ ($0 \le x \le 0.3$) (a) x = 0, (b) x = 0.1, (c) x = 0.2, and (d) x = 0.3 samples demonstrating small polaron hopping behavior.

$$\sigma = \frac{\sigma_0}{T} \exp\left[-\frac{E_{Hop}}{K_B T}\right] \tag{7}$$

where σ_0 is a constant, E_{Hop} is activation energy of small polaron hopping, K_B is Boltzmann constant and T is temperature. If the CSTC system follows the small polaron hopping conduction mechanism then the graph between ln(σT) and $\frac{1}{K_B T}$ should follow the linear relationship and the slope of the curve gives the activation energy of hopping (E_{Hop}) for localized carriers. Fig. 7 depicts the graph between ln(σT) and $\frac{1}{K_B T}$ graph from 300 K to 1050 K. All the CSTC ceramic samples ensues the small polaron hopping conduction mechanism in both the semiconductor regions ($d\sigma/dT > 0$) as shown in Fig. 7. The calculated activation energies (E_{Hop}) for two semiconductor regions are presented in Table 3. It is evident from Table 3 that high temperature semiconductor phase requires lower activation energy compared to room temperature semiconductor phase for all the CSTC compositions. However, in both semiconductor regions, the activation energy for hopping was found to be increased with increasing Ca content in STC, which is evident from the results as shown in Table 3.

Table 3
Activation energy (E_{hop}) of both regions (semiconductor region 1 and semiconductor region 2) calculated from small polaron hopping conduction model using Eq. (7) and fractional small polaron concentration (c) calculated from Eq. (8) for $Ca_xSr_{2-x}TiCoO_6$ ($0 \le x \le 0.3$) ceramic samples.

Composition	E_{hop} (eV) for region 1	E_{hop} (eV) for region 2	Fractional small polaron Concentration (c)
Sr_2TiCoO_6	0.225	0.209	0.44
$Ca_{0.1}Sr_{1.99}TiCoO_6$	0.229	0.224	0.44
$Ca_{0.2}Sr_{1.98}TiCoO_6$	0.235	0.228	0.42
$Ca_{0.3}Sr_{1.97}TiCoO_6$	0.235	0.234	0.42

In 1961 Heikes [55] proposed a formula for Seebeck coefficient (S), when the charge transport is governed by the small polaron hopping, which was later modified by Chaikin and Beni [50] addressing the spin degeneracy of carriers, as expressed below;

$$S = \frac{K_B}{e} \ln\left(\frac{2-c}{c}\right) \tag{8}$$

where c is the fractional concentration of small polaron arising from the multivalent cations present in the system. We estimated the small polaron concentration by using Eq. (8) for all the CSTC samples, which are given in Table 3. It can be seen that the fractional small polaron concentration did not change for Ca doping initially (x = 0.1) but it decreased with higher Ca concentration (x = 0.2 and 0.3) in CSTC systems. This behavior of 'c' values corroborates with the electrical conductivity graph, where, conductivity of x = 0.2 and 0.3 compositions are found to be lower than that of STC.

Furthermore, the thermoelectric power factor ($S^2\sigma$) of $Ca_xSr_{2-x}TiCoO_6$ ($0 \le x \le 0.3$) ceramic samples were estimated from the electrical conductivity and Seebeck coefficient in the temperature range from 300 K to 1050 K as shown in Fig. 8. The highest value of power factor achieved is ~ 5.91 μW/mK^2 at 808 K for (x = 0.1) composition. It can be seen from Figs. 5 and 8 that the power factor is primarily dictated by electrical conductivity as Seebeck coefficient did not change much due to Ca-doping. Lower conductivity obtained for x = 0.2 and 0.3 compositions due to increase in activation energy of hopping as well as decrease in fractional polaron concentration compared to pure STC led to the decrease in power factor. Moreover, power factor did not really increase much for x = 0.1 composition compared to STC, since the increase in electrical conductivity (σ) got somewhat

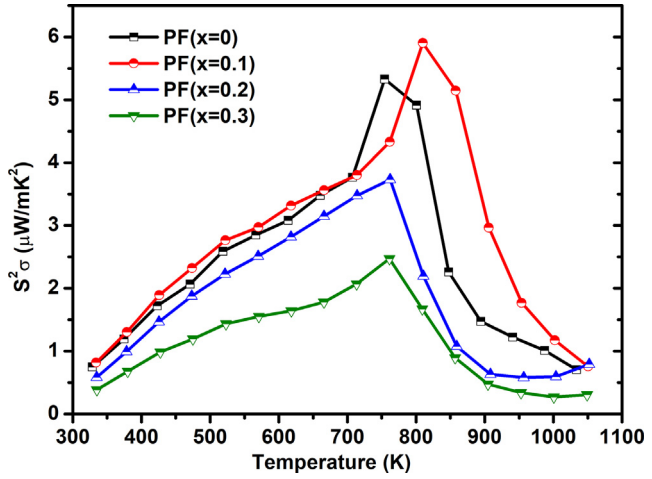

Fig. 8. Thermoelectric power factor ($S^2\sigma$) of $Ca_xSr_{2-x}TiCoO_6$ ($0 \le x \le 0.3$) ceramics.

compensated by the decrease in thermopower (S). A similar type of behavior was also reported in Ca-doped $Sr_{1-x}Ca_xTi_{1-y}Nb_yO_3$[32] perovskite and Sr-doped Ca_2FeMoO_6[33] double perovskite system.

4. Conclusions

We determined the temperature dependent electrical conductivity and Seebeck coefficient of $Ca_xSr_{2-x}TiCoO_6$ ($0 \le x \le 0.3$) double perovskites. Rietveld refinement of XRD data revealed that all the CSTC samples possessed a cubic crystal structure with $Pm\bar{3}m$ space group. The lattice parameter of CSTC ($0 \le x \le 0.3$) was found to be linearly decreased with increase in Ca concentration implying that CSTC system followed Vegard's law. All the CSTC samples exhibited p-type behavior, suggested by a positive Seebeck coefficient obtained in the whole temperature range of measurement from 300 K to 1050 K. X-ray photoelectron spectroscopy (XPS) analysis showed the presence of Co and Ti as lower oxidation states than +4, which is the formal valence of the B-site of the double perovskites resulting the formation of defects like $Co_B^{/}$, $Co_B^{//}$, $Ti_B^{/}$. In the temperature dependent conductivity measurement, all the Ca-doped STC samples manifested an intermediate metallic phase ($d\sigma/dT < 0$) transition between two semiconductors ($d\sigma/dT > 0$) phases. Both semiconductor phases found in all the CSTC samples obeyed the small polaron hopping conduction mechanism.

Acknowledgment

This work is supported by the grant from Science and Engineering Research Board, DST (SERB-DST), India (Grant No: SB/S3/ME/008/2015).

References

[1] S. Twaha, J. Zhu, Y. Yan, B. Li, Renew. Sustain. Energy Rev. 65 (2016) 698–726.
[2] M.H. Elsheikh, D.A. Shnawah, M.F.M. Sabri, S.B.M. Said, M.H. Hassan, M.B.A. Bashir, M. Mohamad, Renew. Sustain. Energy Rev. 30 (2014) 337–355.
[3] X. Zheng, C. Liu, Y. Yan, Q. Wang, Renew. Sustain. Energy Rev. 32 (2014) 486–503.
[4] J. He, Y. Liu, R. Funahashi, J. Mater. Res. 26 (2011) 1762–1772.
[5] G. Mahan, Solid State Phys. 51 (1979) 81–157.
[6] G.A. Slack, CRC Handbook Thermoelectrics (1995) 407–440.
[7] G.J. Snyder, E.S. Toberer, Nat. Mater. 7 (2008) 105–114.
[8] S. Miura, Y. Sato, K. Fukuda, K. Nishimura, K. Ikeda, Mater. Sci. Eng., A 277 (2000) 244–249.
[9] J.P. Heremans, V. Jovovic, E.S. Toberer, A. Saramat, K. Kurosaki, A. Charoenphakdee, S. Yamanaka, G.J. Snyder, Science 321 (2008) 554–557.
[10] K. Peng, X. Lu, H. Zhan, S. Hui, X. Tang, G. Wang, J. Dai, C. Uher, G. Wang, X. Zhou, Energy Environ. Sci. 9 (2016) 454–460.
[11] T. Yin, D. Liu, Y. Ou, F. Ma, S. Xie, J.-F. Li, J. Li, J. Phys. Chem. C 114 (2010) 10061–10065.
[12] I. Terasaki, Y. Sasago, K. Uchinokura, Phys. Rev. B 56 (1997) R12685.
[13] M. Lee, L. Viciu, L. Li, Y. Wang, M. Foo, S. Watauchi, R. Pascal Jr, R. Cava, N. Ong, Nat. Mater. 5 (2006) 537–540.
[14] R. Ishikawa, Y. Ono, Y. Miyazaki, T. Kajitani, Jpn. J. Appl. Phys. 41 (2002) L337.
[15] H. Ohta, K. Sugiura, K. Koumoto, Inorg. Chem. 47 (2008) 8429–8436.
[16] N. Van Nong, N. Pryds, S. Linderoth, M. Ohtaki, Adv. Mater. 23 (2011) 2484–2490.
[17] J. Sun, D.J. Singh, APL Mater. 4 (2016) 104803.
[18] T. Fukushima, A. Stroppa, S. Picozzi, J.M. Perez-Mato, PCCP 13 (2011) 12186–12190.
[19] M. d. C. Viola, M. Martinez-Lope, J. Alonso, P. Velasco, J. Martinez, J. Pedregosa, R. Carbonio, M. Fernandez-Diaz, Chem. Mater. 14 (2002) 812–818.
[20] H. Kato, T. Okuda, Y. Okimoto, Y. Tomioka, Y. Takenoya, A. Ohkubo, M. Kawasaki, Y. Tokura, Appl. Phys. Lett. 81 (2002) 328–330.
[21] R. Cava, B. Batlogg, R. Van Dover, J. Krajewski, J. Waszczak, R. Fleming, W. Peck Jr, L. Rupp Jr, P. Marsh, A. James, Nature 345 (1990) 602.
[22] O.N. Meetei, O. Erten, A. Mukherjee, M. Randeria, N. Trivedi, P. Woodward, Phys. Rev. B 87 (2013) 165104.
[23] O. Erten, O.N. Meetei, A. Mukherjee, M. Randeria, N. Trivedi, P. Woodward, Phys. Rev. B 87 (2013) 165105.
[24] P. Roy, V. Waghmare, T. Maiti, RSC Adv. 6 (2016) 54636–54643.
[25] P. Roy, I. Bose, T. Maiti, Integr. Ferroelectr. 174 (2016) 34–42.
[26] M. Saxena, T. Maiti, Dalton Trans. 46 (2017) 5872–5879.
[27] M. Saxena, P. Roy, M. Acharya, I. Bose, K. Tanwar, T. Maiti, Appl. Phys. Lett. 109 (2016) 263903.
[28] P. Roy, V. Waghmare, K. Tanwar, T. Maiti, PCCP 19 (2017) 5818–5829.
[29] M. Saxena, T. Maiti, Ceram. Int. 44 (2018) 2732–2737.
[30] F. Delorme, C.F. Martin, P. Marudhachalam, D.O. Ovono, G. Guzman, J. Alloy. Compd. 509 (2011) 2311–2315.
[31] Y.-L. Pei, J. He, J.-F. Li, F. Li, Q. Liu, W. Pan, C. Barreteau, D. Berardan, N. Dragoe, L.-D. Zhao, NPG Asia Mater. 5 (2013) e47.
[32] J. Fukuyado, K. Narikiyo, M. Akaki, H. Kuwahara, T. Okuda, Phys. Rev. B 85 (2012) 075112.
[33] T. Sugahara, N. Van Nong, M. Ohtaki, Mater. Chem. Phys. 133 (2012) 630–634.
[34] V.M. Goldschmidt, Naturwissenschaften 14 (1926) 477–485.
[35] M.T. Anderson, K.B. Greenwood, G.A. Taylor, K.R. Poeppelmeier, Prog. Solid State Chem. 22 (1993) 197–233.
[36] J. Rodriguez-Carvajal, Laboratoire Leon Brillouin: CEA-Saclay, France, 2000.
[37] W. Rasband, National Institutes of Health: Bethesda, MD, USA, 1997, 2012.
[38] S. Tougaard, Surf. Sci. 216 (1989) 343–360.
[39] M. Oku, J. Solid State Chem. 23 (1978) 177–185.
[40] T. Chuang, C. Brundle, D. Rice, Surf. Sci. 59 (1976) 413–429.
[41] J. Dillard, D. Crowther, J. Murray, Geochim. Cosmochim. Acta 46 (1982) 755–759.
[42] S.A. Singh, G. Madras, Appl. Catal. A 504 (2015) 463–475.
[43] B. Sexton, A. Hughes, T. Turney, J. Catal. 97 (1986) 390–406.
[44] J.-C. Dupin, D. Gonbeau, H. Benqlilou-Moudden, P. Vinatier, A. Levasseur, Thin Solid Films 384 (2001) 23–32.
[45] O. Lobacheva, Y. Yiu, N. Chen, T. Sham, L. Goncharova, Appl. Surf. Sci. 393 (2017) 74–81.
[46] C. Mousty-Desbuquoit, J. Riga, J.J. Verbist, Inorg. Chem. 26 (1987) 1212–1217.
[47] K. Okada, T. Uozumi, A. Kotani, Jpn. J. Appl. Phys. 32 (1993) 113.
[48] H. Chermette, P. Pertosa, F. Michel-Calendini, Chem. Phys. Lett. 69 (1980) 240–245.
[49] E. Gorham-Bergeron, D. Emin, Phys. Rev. B 15 (1977) 3667.
[50] P. Chaikin, G. Beni, Phys. Rev. B 13 (1976) 647.
[51] H. Kaibe, Y. Tanaka, M. Sakata, I. Nishida, J. Phys. Chem. Solids 50 (1989) 945–950.
[52] P.A. Cox, Transition Metal Oxides: An Introduction to their Electronic Structure and Properties, Oxford University Press, 2010.
[53] N.F. Mott, L. Friedman, Phil. Mag. 30 (1974) 389–402.
[54] S. Li, R. Funahashi, I. Matsubara, K. Ueno, S. Sodeoka, H. Yamada, Chem. Mater. 12 (2000) 2424–2427.
[55] R.R. Heikes, R.W. Ure, Thermoelectricity: Science and Engineering, Interscience Publishers, 1961.